ACS Macro Letters

Letter

pubs.acs.org/macroletters

Morphology Diagram of Single-Layer Crystal Patterns in Supercooled Poly(ethylene oxide) Ultrathin Films: Understanding Macromolecular Effect of Crystal Pattern Formation and Selection

Guoliang Zhang,[†] Xuemei Zhai,[†] Zhenpeng Ma,[†] Liuxin Jin,[†] Ping Zheng,[†] Wei Wang,*[,†] Stephen Z. D. Cheng,*[,‡] and Bernard Lotz*[,§]

[†]Center for Synthetic Soft Materials, The Key Laboratory of Functional Polymer Materials of Ministry of Education and Institute of Polymer Chemistry, College of Chemistry, Nankai University, Tianjin 300071, China

[‡]Department of Polymer Science, College of Polymer Science and Polymer Engineering, The University of Akron, Akron, Ohio 44325-3909, United States

[§]Institut Charles Sadron, 23 Rue du Loess, BP 84047, Strasbourg 67034, France

ABSTRACT: A series of single-layer crystal patterns were observed in ultrathin films of 10 poly(ethylene oxide) fractions of molecular weights ranging from 2.02k to 932.0k g/mol. Morphology transitions between these different crystal patterns were quantitatively identified, and a morphology diagram with respect to supercooling and molecular weight dependencies was constructed. This will foster understanding of the macromolecular effects on the crystal pattern formation and selection critically associated with the parameters of molecular diffusion length and growth anisotropy.

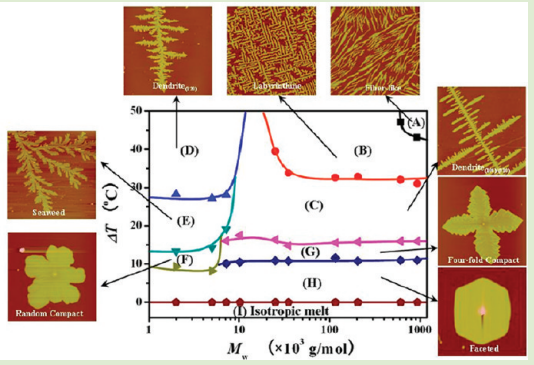

The formation of diverse patterns in a quasi-two-dimensional (2D) space via phase transition is one of the most intriguing phenomena in nature.[1−3] Under such far from thermodynamic equilibrium conditions, labyrinthine, dendritic, seaweed, compact and faceted patterns have been observed in Hele-Shaw flows, electrochemical deposition, directional solidification, and crystalline and magnetic systems.[4−19] Understanding and controlling the microscopic mechanisms underlying these macroscopic patterns formation are of both scientific and practical significance. It has been reported that changes of the patterns are critically associated with growth conditions such as supercooling and anisotropic surface tensions.[20−23] However, no experimentally guided morphology diagram has yet been constructed. This is due to various difficulties in precisely controlling the experimental conditions and the properties of the materials involved.

Polymers such as poly(ethylene oxide) (PEO) are flexible and adjustable in their crystal formation in a wide range of supercoolings ($\Delta T = T_m^0 - T_x$, where T_m^0 is the equilibrium melting temperature and T_x is a crystallization temperature). Flexibility stems from the higher initial nucleation barrier of polymers compared to small molecules.[24,25] Adjustability is linked with anisotropic growth rates (associated with distinct nucleation barriers along the different crystallographic planes) that create different crystal patterns. These growth rates vary with the molecular weight (MW) of polymers. Also, a quasi-2D diffusion of polymer chains in ultrathin films is highly molecular-weight-dependent. Finally, polymer chains kinetically prefer to form single-layer crystals.[15−19,26] Therefore, a systematic study on single-layer crystal patterns using a series of PEO fractions with different MWs in a wide range of ΔT should provide an experimentally observed morphology diagram. This diagram should further provide an opportunity to identify the factors governing the crystal pattern selection and the related transitions.

A total of 10 PEO fractions with MWs ranging between $\bar{M}_w$ = 2.02k and 932.0 kg/mol and with narrow MW distributions ($\bar{M}_w/\bar{M}_n \leq 1.23$) were used in this study. Their molecular characteristics and equilibrium melting temperatures[27] are listed in Table 1. These materials were dissolved in toluene at a concentration of ∼0.015 (wt.) %. Silicon wafers of 0.8 × 0.8 cm^2 in size were treated with Piranha solution of H_2SO_4 (98%)/H_2O_2 (30%) with a ratio of 3:1 in glassware at 120 °C for 30 min to create a layer of -OH groups on the silicon surfaces. These substrates were then cleaned in an ultrasonic water bath. The contact angle of water on the treated silicon wafer was 8°. Ultrathin PEO films were prepared by drop-casting the solution (∼4 μL) onto the silicon surfaces at room temperature. The samples were then dried in vacuum at room temperature for 12 h. The drop-cast method can create an

Received: October 5, 2011
Accepted: December 19, 2011
Published: December 22, 2011

Table 1. Molecular Weight Characteristics and Equilibrium Melting Temperatures of 10 PEO Fractions[a]

samples	$\bar{M}_w$ (g/mol)	$\bar{M}_w/\bar{M}_n$	T_m^0 (°C)
2k-PEO	2020	1.01	53.3
5k-PEO	5050	1.01	62.2
7k-PEO	7200	1.01	64.1
10k-PEO	10000	1.01	65.5
25k-PEO	25000	1.17	67.4
35k-PEO	35000	1.23	67.8
116K-PEO	116000	1.18	68.6
205k-PEO	205000	1.18	68.8
610k-PEO	610000	1.10	69.0
932k-PEO	932000	1.11	69.0

[a] $\bar{M}_w$ and $\bar{M}_w/\bar{M}_n$ were measured using gel permeation chromatography and T_m^0 was calculated according to the equation reported in Ref 27.

ultrathin PEO films with a uniform thickness of about 4 nm. Finally, the as-prepared samples were first heated to 80.0 °C at a rate of 5 °C/min. After a 5 min waiting time (to form a uniformed ultrathin film melt), they were cooled to preset temperatures at the rate of 100 °C/min for crystallization in a period of 5−12 h. A hot-stage multimode atomic force microscope (AFM, Digital Instrumental Nanoscope IV) operated in tapping mode was used to visualize crystal patterns. Crystal patterns were also prepared on the surface of silicone monoxide films supported by copper grid for TEM (Philips Tecnai) observation at an accelerating voltage of 120 kV. Selected area electron diffraction (SAED) experiments were carried out to determine the crystal growth axes and growth planes. The *d*-spacings were calibrated using a TlCl standard.

In our previous studies, we have reported several crystal pattern formed by individual PEO fractions.[15−19] The eight AFM height images in Figure 1 summarize different but typical patterns of the PEO single-layer crystals. A series of TEM bright field images of the crystal patterns and their corresponding SAED data are shown in Figure 2. Figure 1A exhibits edge-on needle-like crystals in which the stems are perpendicular to the substrate normal, as revealed by the *hk*0 SAED pattern in Figure 2A. Figure 1B presents typical labyrinthine crystals, as already observed in our previous work,[18] with growth directions are along the crystallographic *a** and *b* axes. The SAED (Figure 2B) indicates that the PEO stems are parallel to the substrate normal. Figure 1C shows dendritic$_{(100)/(010)}$ crystals with growth directions also along the *a** and *b* axes (SAED in Figure 2C). Figure 1D also displays dendritic$_{(120)}$ crystals, but this time with growth directions along the ⟨120⟩ (SAED in Figure 2D rotated 45° relative to the dendrite branches compared to Figure 2C). Figure 1E shows seaweed crystals with growth directions alternatively along the ⟨120⟩, the *a** and *b* axes (SAED in Figure 2E). A randomly oriented, compact crystal shown in Figure 1F displays multiple growth directions. The patterns displayed in Figure 1C−F were initially observed in the 5k-PEO fraction,[15] and the growth directions were identified recently.[19] Figure 1G displays a 4-fold compact crystal, which was studied in our previous work,[17] with growth directions along the *a** and *b* axes (SAED in Figure 2F). Figure 1H presents a faceted single crystal with a well-defined PEO crystallographic shape limited by two (100) and four {120} planes.[28]

Three order parameters (the peak area obtained from fast-Fourier-transformation (FFT) technique, the branching angle, and the fractal dimension) have been used to quantitatively identify different crystal patterns and elucidate their transition, as shown in Figure 2G−I.[15,17−19] Herein, except for the edge-on needle-like crystals, all crystals are flat-on, and the stems are normal to the crystal basal planes, as indicated by the SAED data (Figure 2B−F). The transition from needle-like-to-labyrinthine crystals is associated with a sudden orientational change of stems in the crystals.[26,29,30] The labyrinthine pattern and the dendritic pattern differ mostly in that the former possesses a periodic structure of the ribbonlike crystals with an identical width on the lateral side of the crystal growth directions, while the latter does not have any periodic features. The FFT technique was used to distinguish two crystal pattern types.[18] The change in the peak area, *A*, obtained from the FFT with ΔT may reliably be used to describe the labyrinthine-dendritic transition, as shown in Figure 2G. In the dendritic to seaweed pattern transition, the growth directions become the feature of interest. The dendrite branches with fixed 90° angle. The seaweed crystals, in our system, grow alternately along three directions with branching angles of 45°. The change in branching angle, θ, with ΔT can be used to assess the transition between dendritic pattern (either (120) or (100)/(010)) and seaweed pattern, as shown in Figure 2H.[15,19] As ΔT decreases further, the dendritic$_{(100)/(010)}$ crystal transforms to a compact, faceted crystal. The dendritic$_{(120)}$, dendritic$_{(100)/(010)}$ and

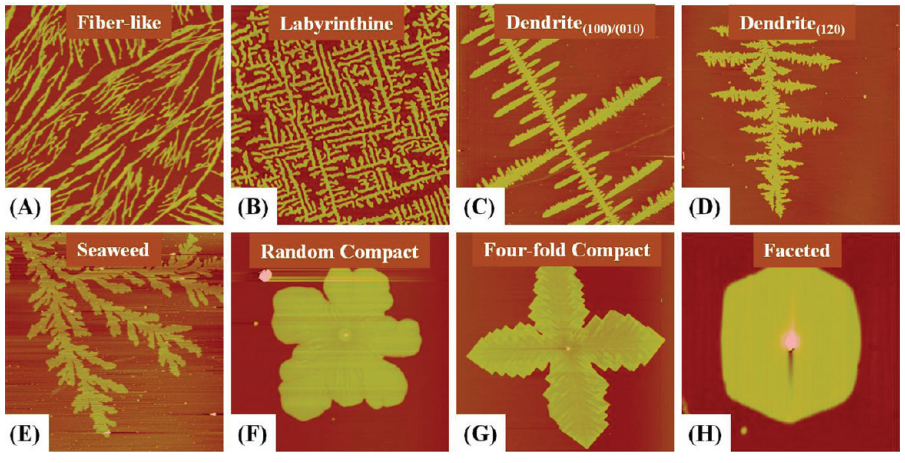

Figure 1. AFM height images showing typical crystal patterns of the PEO single-layer crystals found at different ΔTs for the 10 PEO fractions.

dx.doi.org/10.1021/mz2001109 | ACS Macro Lett. 2012, 1, 217−221

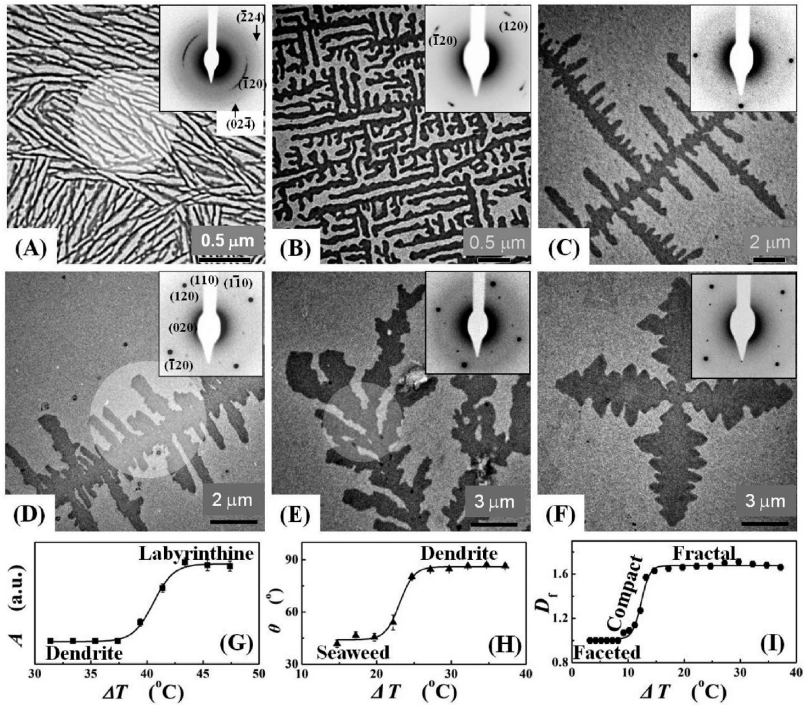

Figure 2. (A–F) TEM bright field images of the different crystal patterns and SAED results; (G) Peak area, A, obtained from FFT analyses to describe labyrinthine-to-dendritic pattern transition; (H) Branching angle, θ, describing the dendritic-to-seaweed pattern transition; (I) Fractal dimension, D_f, describing the transition from the fractal (including dendritic and seaweed) to faceted crystals. The solid lines are fitting results using sigmoidal function.

seaweed crystals all have a similar fractal dimension of ~1.70.[2,3] The 4-fold compact crystal and the randomly compact crystal had fractal dimensions ranging from 1.0 to 1.6. The faceted single crystal has a typical fractal dimension of 1.0. For this reason, the fractal dimension D_f provides a means to quantitatively determine the transitions with ΔT from the dendritic or seaweed to compact crystal and finally, to faceted single crystal, as shown in Figure 2I.[3,15,17,31]

We can construct an experimental morphology diagram of the single-layer crystal patterns of the PEO fractions with respect to ΔT and MW, as shown in Figure 3. Area A

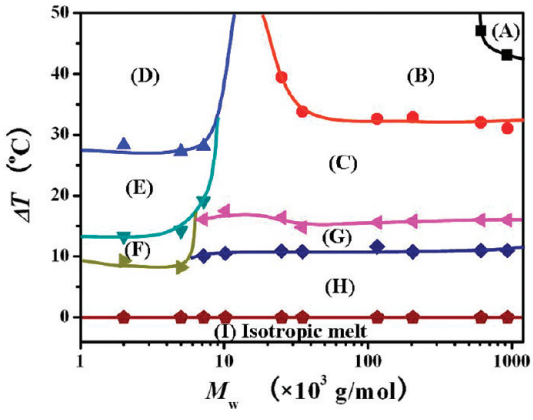

Figure 3. "Morphology diagram" of the PEO single-layer crystal patterns. The letters used correspond to the growth patterns illustrated in Figure 1.

represents the needle-like crystals formed for MW ≥ 610 kg/mol and at $\Delta T \geq 44$ °C. Area B is the labyrinthine crystal pattern for MW ≥ 25 kg/mol and 34 °C ≤ $\Delta T \leq 48$ °C. Area C shows the dendritic$_{(100)/(010)}$ crystal pattern for MW ≥ 7.2 kg/mol and ≈16 °C ≤ $\Delta T \leq 34$ °C. Area D represents the dendritic$_{(120)}$ crystal pattern for MW ≤ 7.2 kg/mol and $\Delta T >$ 29 °C. Area E is the seaweed crystal pattern (MW ≤ 7.2 kg/mol and 15 °C < $\Delta T \leq 29$ °C). Area F shows the randomly compact crystal pattern for MW ≤ 5 kg/mol and 10 °C < $\Delta T \leq 15$ °C. Area G is the 4-fold compact crystal pattern grown for MW ≥ 7.2 kg/mol and 11 °C < $\Delta T \leq 16$ °C. Finally, area H represents the faceted crystals observed for the whole MW range in this investigation within 0 °C < $\Delta T \leq 11$ °C. Note that sharp transition boundaries delineate the different crystal patterns in this morphology diagram.

The growth anisotropies of the crystal patterns exhibit strong MW dependence. For the PEO fractions with MW ≤ 7.2 kg/mol, crystals have dendritic$_{(120)}$, seaweed, randomly compact (except for MW = 7.2 kg/mol), and faceted crystal patterns. The crystal growth directions changed from the ⟨120⟩ to the a^* and b axes as ΔT decreases. The dendritic$_{(120)}$–seaweed transition occurrs because of changes in crystal growth from 1D to 2D geometry.[19] For the PEO fractions with MW > 10 kg/mol, the flat-on crystals take on the labyrinthine, dendritic$_{(100)/(010)}$, 4-fold compact, and faceted patterns as ΔT decreases. No seaweed or randomly compact patterns are observed, and the crystal growth direction remain along the a^* and b axes throughout the ΔT range studied when MW ≥ 10 kg/mol.

Despite the crystalline anisotropy, three types of major crystal pattern transitions take place as ΔT decreases: needle-like to labyrinthine, labyrinthine to fractal, and fractal to faceted via compact. The formation of edge-on crystals in area A and the flat-on crystals in the rest of the areas reflect different mechanisms controlling the crystallization of PEOs. The differences between the interfacial energies γ_{cs} between the

dx.doi.org/10.1021/mz2001109 | ACS Macro Lett. 2012, 1, 217–221

crystal and the substrate and γ_{ms}, that is, between the melt and the substrate, are likely to play a key role.[32] When $\gamma_{ms} > \gamma_{cs}$, the primary nuclei favor an edge-on orientation but the growing lamellae tend toward a flat-on mode to form larger lateral size crystals covering the substrate surface in order to minimize the interfacial energy. The crystal growth rates of PEOs with MW $\geq$ 610 kg/mol are quite slow at $\Delta T \geq 44$ °C when compared to other fractions with lower MWs. The edge-on lamellae observed are immature crystals that has not enough time to develop into large PEO crystals. The flat-on crystals, found in the rest of the areas, are matured lamellae. This orientational change is consistent with observations in other crystalline polymeric thin films.[32−34]

Crystal growth in ultrathin films is associated with, and results from, quasi-2D diffusion of the chain molecules.[26] The changes in molecular diffusion length, λ, may explain the selection of specific growth patterns and thus the corresponding pattern transitions. The values of λ were found to be strongly dependent on the diffusion coefficients of supercooled PEO chains, D, and their crystal growth rates, v. This dependence is expressed in the scaling law role of $\lambda \propto D/v$.[2,35,36] The crystal width, W, is also proportional to the D/v.[8,35] Therefore, changes in W reflect the variation of λ with ΔT. These changes are plotted in Figure 4A.

It is well established that D increases and v decreases with decreasing ΔT.[24,37] At high ΔTs, D is small, but v is large. Therefore, both λ and W are small. For edge-on needle-like crystals, W is ∼10 nm. As ΔT decreases, D increases and v decreases slightly. The combined variations result in increases in λ and W. The width of flat-on labyrinthine crystals increases to ∼40 nm.

Labyrinthine crystals form because λ remains small at relatively high ΔTs. The chain diffusion in the supercooled melt takes place within less than one micrometer in front of the crystal growth tip. Thus, the local diffusion of chains governs the formation of the labyrinthine crystal.[18] As ΔT decreases further, the chain diffusion becomes progressively delocalized and the crystal growth rate decreases, Both variations lead to a gradual increase of λ, while W increases by about 1 order of magnitude from ∼200 nm to 1.5−2.5 μm. The diffusion-limited-aggregation (DLA) mechanism controls the formation of fractal crystals in this way.[38,39]

When ΔT decreases to ∼17.0 °C, we note that W increases dramatically. This trend is continuous with decreasing ΔT, as shown in Figure 4A. The trend in λ would also be continuous, and the PEO chains would progressively have the possibility to diffuse over sufficient distance to reach the growing crystal fronts. In this case, the impact of the *limitation* of the DLA mechanism is gradually reduced, and the surface nucleation on the growth front sets the limits to crystal growth.[15,17] In short, the PEO chains have enough time and thermal energy for surface diffusion to take place and they adjust their conformations when reaching the crystal growth front.[5] The number of re-entry corners in the crystals decreases with decreasing ΔT. As a result, the crystal patterns change from fractal crystals to compact structures to faceted single crystals, indicating that the nucleation-limited-growth (NLG) becomes dominant. In this process, as shown in Figure 4C, the value of the fractal dimension, D_f, decreases gradually from ∼1.70, the typical value for 2D fractal patterns, to approximately 1.00 for faceted single crystals.[15,17,31]

For all the PEO fractions studied, D_f has an inflection point at $\Delta T = 13.6 \pm 0.3$ °C (Figure 4C). This value is in the middle

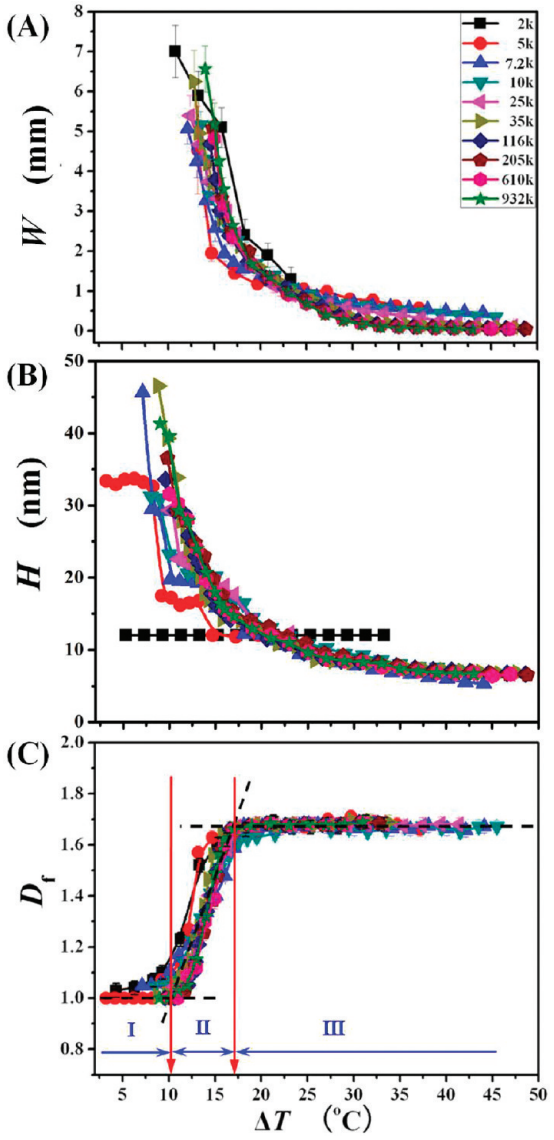

Figure 4. Plots of crystal width W vs ΔT (A), crystal thickness H vs ΔT (B), and fractal dimension D_f vs ΔT (C) for different PEO fractions.

region of the so-called growth regime II determined in PEO bulk crystallization.[26] Crystal thickness, H, for the PEO fractions with MW $\geq$ 10k g/mol is about 20 nm for both the bulk and in ultrathin film samples at $\Delta T \approx 13.6$ °C, as shown in Figure 4B. The supercooling of 13.6 °C may well be a characteristic value for PEO crystallization in both the bulk and the ultrathin films. When $\Delta T > 13.6$ °C, the crystal thickness is less than 20.0 nm thick, and the nucleation barrier is low, so molecular diffusion (or the DLA mechanism) control crystal growth and pattern formation. When $\Delta T < 13.6$ °C, the crystal thickness is over 20.0 nm, and the nucleation barrier is high, so surface nucleation (or the NLG mechanism) governs the crystallization and resulting morphologies. For lamellar thicknesses in the vicinity of 20 nm, the coupling of DLA and NLG create intermediate patterns, such as compact crystals. Consequently, we can roughly divide the $D_f \sim \Delta T$ curve into three regimes (Figure 4B). Regime II/III transitions appeared at $\Delta T = 17.0 \pm 0.7$ °C and regime I/II transitions appeared at $\Delta T = 10.4 \pm 0.6$ °C. The boundaries of the three

dx.doi.org/10.1021/mz2001109 | *ACS Macro Lett.* 2012, 1, 217−221

regimes are consistent with the three regimes obtained in bulk PEO crystallization.[27,40] Therefore, this may be another method to indentify the three regimes of PEO crystallization in ultrathin films.

Finally, due to the long-chain nature of PEOs, the diffusion length and crystal morphology and aspect ratio can be tuned by varying MWs at constant ΔT. For instance, the diffusion coefficients of PEOs obey the scaling law $D \propto M^{-1.5}$, where M is molecular weight, in quasi-2D thin films.[41] In an earlier study, we have found $W \propto M^{-0.24}$, where W is proportional to the labyrinthine crystal width.[18] In other words, the crystalline anisotropy of the PEO labyrinthine crystals increases with increasing the MW. In addition, ΔT can be adjusted to produce different crystal patterns at a constant MW. It is evident that systematic studies, such as this one, are prerequisites to understand single-layer crystal pattern formation and transition.

In summary, an experimentally observed morphology diagram of single-layer crystal patterns has been generated for a series of PEO fractions crystallized over a broad ΔT range in ultrathin films. Various crystal patterns including needle-like, labyrinthine, dendritic, seaweed, compact, and faceted have been found. These crystal patterns exhibit ΔT and MW dependencies. Transitions between the different crystal patterns were quantitatively identified based on fractal dimensions and crystal aspect ratios. The pattern selections were qualitatively interpreted in terms of competition between the diffusion coefficients of PEO chains and their growth rates. These results should be of interest in further theoretical and experimental investigations dealing with the formation and selection of specific crystal pattern.

AUTHOR INFORMATION

Corresponding Author

*E-mail: weiwang@nankai.edu.cn (W.W.); scheng@uakron.edu (S.Z.D.C); bernard.lotz@ics-cnrs.unistra.fr (B.L).

Notes

The authors declare no competing financial interest.

ACKNOWLEDGMENTS

This project was supported by the National Natural Science Foundation of China for a grant (Grants NSFC20474033 and 20874053) to support this work. The portion of our research at the University of Akron was supported by U.S. National Science Foundation (DMR-0906898).

REFERENCES

(1) Langer, J. S. *Rev. Mod. Phys.* **1980**, *52*, 1.
(2) Meakin, P. *Fractals, Scaling and Growth Far from Equilibrium*; Cambridge University Press: Cambridge, 1997.
(3) Ball, P. *The Self-Made Tapestry: Pattern Formation in Nature*; Oxford University Press: New York, 2001.
(4) Rosensweig, R. E.; Zahn, M.; Shumovich, R. *J. Magn. Magn. Mater.* **1983**, *39*, 127.
(5) Vicsek, T. *Phys. Rev. Lett.* **1984**, *53*, 2281.
(6) Ben-Jacob, E.; Garik, P. *Nature (London)* **1990**, *343*, 523.
(7) Hwang, R. Q.; Schröder, J.; Günther, C.; Behm, R. *Phys. Rev. Lett.* **1991**, *67*, 3279.
(8) Reiter, G.; Sommer, J. U. *Phys. Rev. Lett.* **1998**, *80*, 3771.
(9) Hutter, J. L.; Bechhoefer, J. *Phys. Rev. Lett.* **1997**, *79*, 4022.
(10) Provatas, N.; Wang, Q. Y.; Haataja, M.; Grant, M. *Phys. Rev. Lett.* **2003**, *91*, 155502.
(11) Sandnes, B.; Knudsen, H. A.; Måløy, K. J.; Flekkøy, E. G. *Phys. Rev. Lett.* **2007**, *99*, 038001.
(12) Li, S.; Lowengrub, J. S.; Fontana, J.; Palffy-Muhoray, P. *Phys. Rev. Lett.* **2009**, *102*, 174501.
(13) Singer, H. M.; Singer, I.; Bilgram, J. H. *Phys. Rev. Lett.* **2009**, *103*, 015501.
(14) Shcherbina, M. A.; Ungar, G. *Macromolecules* **2007**, *40*, 402.
(15) Zhai, X.; Wang, W.; Zhang, G.; He, B. *Macromolecules* **2006**, *39*, 324.
(16) Ma, Z.; Zhang, G.; Zhai, X.; Jin, L.; Tang, X.; Zheng, P.; Wang, W. *Polymer* **2008**, *49*, 1629.
(17) Zhang, G.; Jin, L.; Ma, Z.; Zhai, X.; Yang, M.; Zheng, P.; Wang, W.; Wegner, G. *J. Chem. Phys.* **2008**, *129*, 224708.
(18) Zhang, G.; Jin, L.; Zheng, P.; Shi, A.-C.; Wang, W. *Polymer* **2010**, *51*, 554.
(19) Zhang, G.; Cao, Y.; Jin, L.; Zheng, P.; Van Horn, R. M.; Lotz, B.; Cheng, S. Z. D.; Wang, W. *Polymer* **2011**, *52*, 1133.
(20) Brener, E.; Müller-Krumbhaar, H.; Temkin, D. *Europhys. Lett.* **1992**, *17*, 535.
(21) Brener, E.; Müller-Krumbhaar, H.; Temkin, D. *Phys. Rev. E* **1996**, *54*, 2714.
(22) Brener, E.; Müller-Krumbhaar, H.; Temkin, D. *Phys. A* **1998**, *249*, 73.
(23) Hoyt, J. J.; Asta, M.; Karma, A. *Mater. Sci. Eng.* **2003**, *R41*, 121.
(24) Wunderlich, B. *Macromolecular Physics*; Academic: New York, 1976; Vol. *1*−*3*.
(25) Cheng, S. Z. D. *Phase Transitions in Polymers: The Role of Metastable States*; Elsevier Science: New York, 2008.
(26) Liu, Y.-X.; Chen, E.-Q. *Coord. Chem. Rev.* **2010**, *254*, 1011.
(27) Cheng, S. Z. D.; Chen, J.; Janimak, J. J. *Polymer* **1990**, *31*, 1018.
(28) Lotz, B.; Kovacs, A. J. *Kolloid Z. Z. Polym.* **1966**, *209*, 97.
(29) Schönherr, H.; Frank, C. W. *Macromolecules* **2003**, *36*, 1188.
(30) Wang, Y.; Rafailovich, M.; Sokolov, J.; Gersappe, D.; Araki, T.; Zou, Y.; Kilcoyne, A. D.; Ade, H.; Marom, G.; Lustiger, A. *Phys. Rev. Lett.* **2006**, *96*, 028030.
(31) Mandelbrot, B. B. *The Fractal Geometry of Nature*; W. H. Freeman and Company: San Francisco, 1982.
(32) Wang, Y.; Ge, S.; Rafailovich, M.; Sokolov, J.; Zou, Y.; Ade, H.; Lüning, J.; Lustiger, A.; Marom, G. *Macromolecules* **2004**, *37*, 3319.
(33) Li, L.; Chan, C.-M.; Yeung, K. L.; J.-H., L.; Ng, K.-M.; Lei, Y. *Macromolecules* **2001**, *34*, 316.
(34) Wang, Y.; Chan, C.-M.; Ng, K.-M.; Li, L. *Macromolecules* **2008**, *41*, 2548.
(35) Keith, H. D.; Padden, F. J. *J. Appl. Phys.* **1964**, *35*, 1270.
(36) Mullins, W. W.; Sekerka, R. F. *J. Appl. Phys.* **1964**, *35*, 444.
(37) Rubinstein, M.; Colby, R. *Polymer Physics*; Oxford University Press: New York, 2003.
(38) Witten, T. A.; Sander, L. M. *Phys. Rev. Lett.* **1981**, *47*, 1400.
(39) Witten, T. A.; Sander, L. M. *Phys. Rev. B* **1983**, *27*, 5686.
(40) Hoffman, J. D.; Miller, R. L. *Polymer* **1997**, *38*, 3151.
(41) Sukhishvili, S. A.; Chen, Y.; Müller, J. D.; Gratton, E.; Schweizer, K. S.; Granick, S. *Macromolecules* **2002**, *35*, 1776.